Integrated micro-optical imaging system with a high interconnection capacity fabricated in planar optics

Stefan Sinzinger and Jürgen Jahns

An integrated free-space optical interconnection system with 2500 parallel data channels is demonstrated. The design is based on a combination of microchannel imaging and conventional imaging. A modification of the hybrid imaging configuration allows one to achieve optimized image quality over large image fields. © 1997 Optical Society of America

Key words: Micro-optics, optical interconnections, aberrations, integrated optics.

1. Introduction

Optical interconnects are widely discussed as a solution for communication bottlenecks of VLSI electronics. Besides the high temporal bandwith of optical interconnects, the high degree of parallelism of free-space optics is promising for providing the necessary data throughput.[1,2]

Free-space optical interconnects are implemented by the imaging of arrays of output devices onto detector arrays. In communication applications the small optical windows of the input–output (I/O) arrays generally are not densely packed but are distributed at discrete positions over the image field. High resolution is needed to resolve the I/O windows, but the area between the windows is black or optically uninteresting. Such device arrays are often called dilute arrays.[3] Typical examples for dilute arrays are arrays of electronic logic gates with optical I/O's, also called smart-pixel arrays,[4] or bundles of optical fibers.

For optimum performance, the optical imaging system has to be adjusted to this specific situation. A conventional imaging system provides constant resolution over an extended image field, regardless of the influence of aberrations [Fig. 1(a)]. This constitutes a waste of the space–bandwidth product if only distinct islands of the image field are of interest. Therefore it has been suggested using arrays of microlenses, each transmitting one single channel.[5] This approach is often called microchannel imaging. In this case, however, the interconnection distance is limited by diffraction at the microlens pupils.[6]

Hybrid imaging is a combination of microchannel and conventional imaging.[3,7–11] Microlens arrays are used to collimate the light from the sources (A1) and to focus the light to the detectors (A2) [Fig. 1(b)]. In order to avoid cross talk because of the diffraction at the microlens pupils, an additional imaging step between the planes of the microlenses is used. This combination allows one to distribute the space–bandwidth product of the imaging lenses precisely as needed for dilute arrays. The high resolution is provided locally by the microlenses. This imaging concept is particularly interesting for the design of planar-integrated free-space optics[12] because it also reduces aberrations. In planar optics the optical system is folded into a two-dimensional geometry and is integrated monolithically, e.g., by diffractive optical elements (DOE's). The propagation along the oblique optical axis puts additional constraints on the design of the DOE's.

In an earlier experiment, an integrated hybrid imaging system with 1024 parallel channels was demonstrated.[13] It has been shown in Ref. 13 that systems with even more channels can be achieved if all available design parameters are used to optimize the optical performance.

To this end we use the design freedom offered by parameters such as focal length and deflection angle of the lenslets in the array A1 and A2. The basic idea is presented in Section 2. It leads to a modified hybrid imaging system. In Section 3 we show ex-

The authors are with the Optische Nachrichtentechnik, Fern Universität, Feithstrasse 140, 58084 Hagen, Germany.

Received 16 September 1996; revised manuscript received 11 February 1997.

0003-6935/97/204729-07$10.00/0

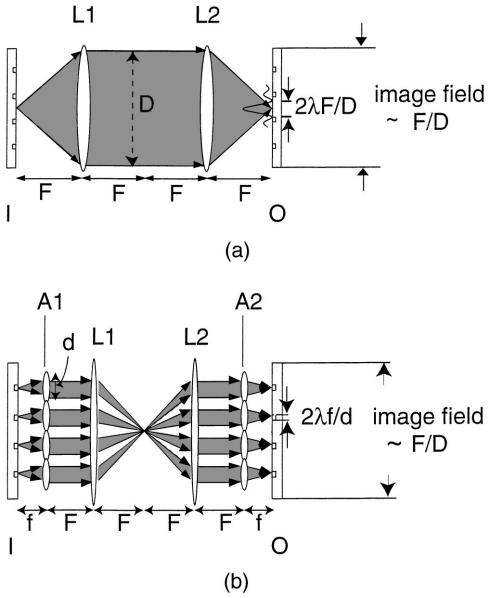

Fig. 1. Imaging setups for the implementation of optical interconnects (I's, input arrays; O's, detector arrays; L1 and L2, imaging lenses with focal length F and diameter D): (a) conventional $4F$ imaging, (b) hybrid imaging (A1, A2, uniform arrays of microlenses with focal length f and diameter d).

perimental results of such a hybrid imaging system with 2500 parallel channels. In Section 4 we discuss the limitations of the system as well as alignment tolerances. In Section 5 a space-variant hybrid imaging system is suggested as a specific application of the modified hybrid imaging scheme.

2. Modified Hybrid Imaging Configuration

In the conventional hybrid imaging configuration [Fig. 1(b)] uniform arrays of microlenses (A1 and A2) are used. The imaging of A1 and A2 onto each other needs to be performed by a telecentric $4F$ setup. Telecentricity is required in order to avoid dislocation and distortion of the image spots. The use of uniform lenslet arrays therefore is not perfect in terms of the optical design and limits the systems performance to space-invariant one-to-one imaging.

More design flexibility can be achieved if the microlenses of arrays A1 and A2 not only collimate the light but also deflect it[9] [Fig. 2(a)]. If at the same time the focal length of each microlens is adjusted individually [Fig. 2(b)] we can optimize the hybrid imaging setup. Instead of a $4F$ configuration being used, a single imaging lens in plane L is used as a field lens that images the entrance pupils in A1 onto the exit pupils in A2. Below we call this modified hybrid setup, the hybrid $2F/2F$ configuration, as opposed to the conventional hybrid imaging configuration that we call the hybrid $4F$ setup.

The fabrication of lenslet arrays in which the focal length as well as the deflection angle of each microlens is designed individually might seem to require additional technological effort. This is, however, not necessarily the case. For our experiments, e.g., we

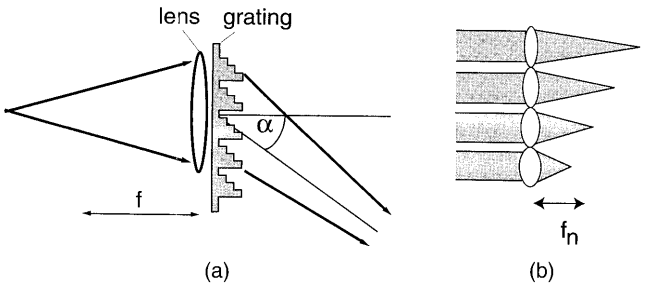

Fig. 2. Additional degrees of freedom that are used for the optimization of the imaging quality: (a) deflection angle introduced by the individual microlenses, (b) variable focal lengths of the individual microlenses.

used multilevel DOE's that offer the necessary design freedom without increasing the complexity of the fabrication process. To improve the performance of the DOE's further we recently suggested using efficient detour-phase holograms in which the beam deflection results naturally from the use of a carrier grating.[14] Other possible implementations use doublet elements such as hybrid diffractive–refractive elements,[6,15] as indicated in Fig. 3. Beam deflection can also be achieved with uniform lenses that are shifted locally to achieve the desired beam deflection.[16]

The main advantage of the hybrid $2F/2F$ configuration is that we are able to optimize the imaging properties for each individual channel by the individual design of each microlens. To this end it is necessary to design each of the microlenses of A1 and A2 for the imaging of a single source in plane I onto the center of the imaging lens L. As is well known, for a single point source ideal imaging can be achieved by proper optical design. The focal lengths of the optimized microlenses depend on their positions within the array. We use the indices n and m to indicate this position in the x and the y directions, respectively. The center of the microlens (n, m) is located at $[(n - 0.5)d, (m - 0.5)d]$, where d is the diameter of the microlenses and the origin of the coordinate

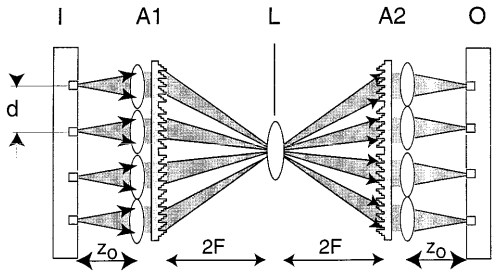

Fig. 3. Optimized $2F/2F$ hybrid imaging system with deflecting microlens arrays A1 and A2 and one field lens L with focal length F.

system is located on the optical axis. Different focal lengths result for the x and the y directions:

$$f_x(n) = \frac{z_o[(n-0.5)^2 d^2 + 4F_x^{\,2}]^{1/2}}{z_o + [(n-0.5)^2 d^2 + 4F_x^{\,2}]^{1/2}}, \quad (1)$$

$$f_y(m) = \frac{z_o[(m-0.5)^2 d^2 + 4F_y^{\,2}]^{1/2}}{z_o + [(m-0.5)^2 d^2 + 4F_y^{\,2}]^{1/2}}. \quad (2)$$

In Eqs. (1) and (2), z_o is the object distance between planes I and A1 (Fig. 3). F_x and F_y denote the focal lengths of the imaging lens in plane L. In the case of an oblique optical axis, e.g., in planar-integrated systems, this lens is optimized for the imaging along the oblique axis.[13] This optimization effectively results in different focal lengths for the x and the y directions ($F_x \neq F_y$). In combination with the deflection angle that can be derived from geometric considerations, Eqs. (1) and (2) yield the phase profile of the individual microlenses in A1 and A2. The required elements can be implemented as computer-generated DOE's. Aberrations such as field curvature, astigmatism, and coma can be completely eliminated in this optimized system.

In the hybrid $2F/2F$ imaging setup, the only possible aberrations stem from the imaging step that images A1 onto A2. However, these aberrations are smaller than those in hybrid $4F$ imaging. Their magnitude decreases with the numerical aperture of the imaging lens. The minimum diameter of lens L can be calculated from the lateral extension of the images of the sources in plane L. According to the design of the focal lengths the images of the sources at the very edge ($n = N_x$ and $m = N_y$) of the array have the largest diameter. This size of the images in plane L determines the minimum diameter of the imaging lens. The diameter D_x of the lens in the x direction can be calculated from

$$D_x = \left(\frac{N_x^{\,2}}{4} d^2 + 4F_x^{\,2}\right)^{1/2} 2\frac{\lambda}{d}. \quad (3)$$

Here N_x represents the number of sources in the x direction with pitch d in source array I and F_x is the focal length of the imaging lenses. The pitch d also corresponds to the diameter of the microlenses.

For large interconnection distances ($F_x \gg d$) D_x is considerably smaller than the diameter of the imaging lenses (L1 and L2) in the conventional or the hybrid $4F$ case.[8] This results in a reduction of the numerical aperture of the imaging lens, which in turn results in a reduction of the aberrations.

3. Experimental Implementation of a Hybrid $2F/2F$ Imaging System

We have fabricated a hybrid $2F/2F$ imaging system in a planar optical configuration.[17] The setup is shown schematically in Fig. 4. An array of 50×50 microlenses is used to couple the light into the glass substrate. Except for the microlens arrays, the surfaces of the glass substrate are reflection coated. The light propagates along a zig-zag path (oblique angle $\alpha = 10.15°$) within the fused-silica glass substrate of thickness $t = 6$ mm. The microlenses of arrays A1 and A2 are individually designed to focus the light in plane L, where the imaging lens is located. The imaging lens was designed for imaging along the oblique optical axis.[13] The microlenses of A1 and A2 (diameter $d = 50$ μm, numerical aperture ≈0.11) and the imaging lens L (diameter $D = 897$ μm, numerical aperture 0.037) were fabricated lithographically as four-level DOE's. The system demonstrates 50×50 parallel data channels with an interconnection density of 400 mm^{-2}. The lateral interconnection distance s was 8.6 mm.

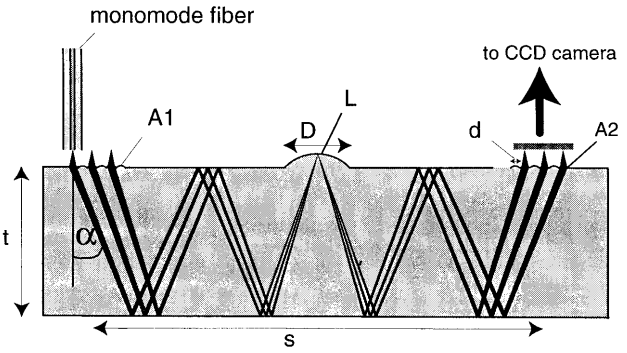

Fig. 4. Schematic of the experiment that demonstrates the planar optical imaging setup with 2500 parallel data channels (A1, A2, optimized microlens arrays; L, imaging lens; substrate thickness $t = 6$ mm; interconnection length $s = 8.6$ mm).

For reasons of mask economics only 257 of the 2500 possible channels were actually realized. Their positions are indicated in Fig. 5. For a light source we used an optical fiber with a core diameter of 8.5 μm. The channels were tested individually. Figures 6(a) and 6(b) show multiple-exposure photographs taken with a CCD camera of sections at the center and the edge of the output plane, respectively. A scan through the corresponding pictures shows the profile of the focal spot (Fig. 7). The image quality was uniform over the whole array. We measured a diameter of $w \approx 19.2$ μm for the images of the fiber

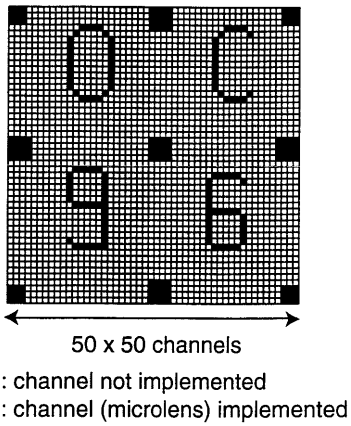

Fig. 5. Schematic of the input array of 50×50 microlenses marking the actually implemented channels.

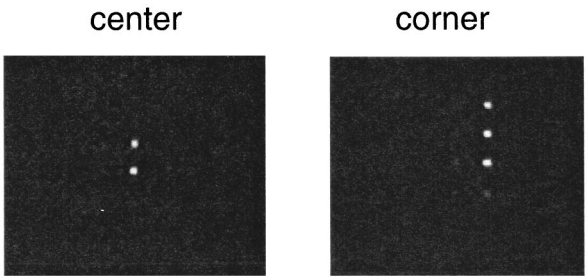

Fig. 6. Multiple-exposure photographs of the images of the fiber tip, imaged sequentially by (a) two channels in the center of the planar optical imaging system, (b) three channels at the edge of the image field.

core. This is larger than the size of the diffraction-limited focus, which is $w_d \approx 7.73$ μm. The extended spot diameter can be explained by the spectral bandwidth of the 850-nm laser diode that was used in our experiment and by the multimode properties of the fiber at this wavelength. During the experiment we observed some stray light, which reduces the contrast ratio to ~1:10. It has been shown previously that contrast ratios better than 1:200 can be achieved if absorption layers are used in the areas between the optical elements.[13] Because of the oblique optical axis in planar optics, most of the stray light propagates into directions where it can be stopped by suitable absorption layers. In our configuration we therefore expect a contrast improvement of at least a factor of 10 to values better than 1:100.

4. Power Budget

The goal in our experiment was to demonstrate that the hybrid $2F/2F$ configuration allows one to achieve good image quality over large image fields. Therefore the system was not optimized with respect to light efficiency. Nevertheless an estimation of the efficiency of the individual channels is interesting for a future optimization. For the calculation we use the efficiency values resulting from scalar diffraction theory. This should be valid in our case, as the lithographic minimum feature was considerably larger than the wavelength. The incoupling microlenses were implemented as binary DOE's with an efficiency of $\eta_c \approx 0.4$. Imaging lens L was implemented as a four-phase-level DOE with an efficiency of $\eta_L \approx 0.81$. Additional Fresnel reflection losses of ~5% occur during the incoupling and outcoupling of the light ($\eta_F = 0.95$). Another important effect that reduces the efficiency stems from the reflections inside the substrate. In our system the light propagates along four zig-zag bounces so that seven reflections at mirrors on the glass surfaces are required. For our experiment we used aluminum coatings with a reflectivity of only ~85% at $\lambda = 850$ nm to fabricate the mirrors ($\eta_R = 0.85$). This results in an overall efficiency η for the individual channel:

$$\eta = \eta_R{}^7 \eta_c{}^2 \eta_L \eta_F{}^2 = 3.75\%. \quad (4)$$

The two main reasons for this low efficiency are the reflectivity of the mirrors as well as the incoupling lenses. Metallic layers with higher reflectivity can be used instead of the aluminum coating for the fabrication of the mirrors. With the use of silver coatings ($\eta = 0.98$), e.g., the efficiency can already be increased to $\eta > 10\%$. The use of dielectric coatings for mirrors with even higher reflectivities is currently being investigated.

A significant gain in efficiency can be achieved from an improvement of the efficiency of the incoupling lenslet arrays. Improved lithography allows the fabrication of multilevel DOE's with higher efficiency, even for the high deflection angles needed for large systems. Additional improvement can be expected from the use of the detour phase as an additional degree of freedom for efficient DOE's.[14] Overall efficiencies of 20%–50% per channel seem feasible with the approach. Because all the channels consist of the same components that are all fabricated in the same lithographic process a good uniformity in the efficiency over the individual channels can be expected.

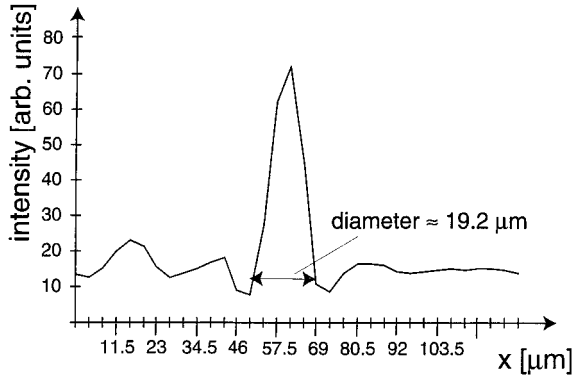

Fig. 7. One-dimensional intensity distribution of one of the focal spots shown in Fig. 6.

5. Systems Considerations

A. Estimation of the Maximum Number of Channels

We now estimate the maximum number of data channels that can be implemented with such a hybrid $2F/2F$ setup integrated in planar optics. As in the demonstration experiment, we assume the use of DOE's. Therefore the number of channels is limited by the maximum deflection angle determined by the minimum feature size of the lithographic fabrication process.

We first consider the x direction that corresponds to the direction in which the system is folded. As a geometric boundary condition for planar optics the light originating from the left edge of the array must not overlap with the right edge of the array after one zig-zag propagation in the substrate. Taking into account the size of the input array as well as the

diffraction blur, we find a condition for the lateral shift Δx after one zig-zag bounce:

$$\Delta x \geq N_x d + \frac{\lambda}{d}(N_x^2 d^2 + 4t^2)^{1/2}. \quad (5)$$

We can calculate the necessary propagation angle:

$$\tan(\alpha_x) = \frac{\Delta x}{2t}. \quad (6)$$

With the parameters used in our experiment (N_x = 50, d = 50 μm, t = 6 mm), relation (5) and Eq. (6) yield a deflection angle of $\alpha_x = 12.7°$. In addition we need to take into account the divergence angle α_{div} of the light in front of the microlens. A typical value for a 850-nm vertical-cavity surface-emitting laser diode with an output window of δ = 10 μm is $\alpha_{\text{div}} = 4.9°$. Thus the maximum deflection angle introduced by a diffractive element in our example would be $\alpha_{\max} = 17.6°$. According to the equation

$$\sin(\alpha_{\max}) = \frac{\lambda}{nLw_{\min}}, \quad (7)$$

we can calculate a necessary minimum feature size of $w_{\min}$ = 0.96 μm for the fabrication process if diffractive elements with two phase levels (L = 2) are used. L denotes the number of phase levels of the element, and n is the refractive index of the substrate (n = 1.46 SiO_2).

UV lithography with minimum features sizes in the submicrometer range allows the fabrication of systems optimized for even larger arrays. For the implementation of 100 parallel channels in the x direction, for example, a maximum deflection angle of $\alpha_{\max} = 28.4°$ is necessary, which corresponds to a minimum feature size of $w_{\min}$ = 0.61 μm.

In the y direction the requirements are less stringent because the optical axis is not inclined in this direction. If the light has to be focused in the center of the configuration, a deflection angle α_y is sufficient in addition to the diverging angle α_{div}:

$$\alpha_y = \arctan\left[\frac{(N_y/2)/d}{2t}\right]. \quad (8)$$

A comparison of Eq. (6) and Eq. (8) shows that the number N_y of channels in the y direction can be more than two times as large as N_x for a given minimum feature size.

These estimations show that, for a channel pitch of 50 μm, as many as 100 × 200 channels can be interconnected with the hybrid $2F/2F$ imaging configuration. In this estimation we used somewhat arbitrary but realistic parameters for the smart-pixel devices. It is straightforward to perform the same calculation for the specifications of any of the device arrays available nowadays. Because the achievable diffraction angles determine the maximum size of the image field, the channel pitch has a direct influence on the channel capacity. Typically device arrays are built on a 62.5- or a 125-μm grid in order to match the channel spacing of densely packed monomode fibers. In this case the channel capacity of the imaging configuration reduces to 80 × 160 or 40 × 80 channels, respectively.

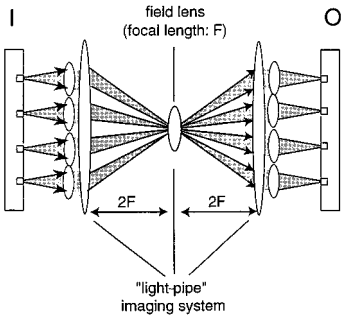

Fig. 8. Hybrid imaging configuration in which a three-lens light pipe is used for the imaging between the planes of the microlens arrays.

B. System Tolerances

Important aspects of the systems design are the tolerances of the system with respect to the various possible misalignment errors and deviations from the design parameters. In the planar optical realization, relative misalignments of the optical components can be neglected because of the lithographic fabrication process that yields submicrometer precision. However, substrate tolerances as well as wavelength or temperature variations need to be considered.[18] Below we compare the tolerances of the hybrid $2F/2F$ imaging system with the hybrid $4F$ configuration. We consider a planar optical realization of the system. All the optical elements are designed for a specific design wavelength and implemented as DOE's on the surface of a glass substrate.

In a planar optical system the optoelectronic devices are integrated with the optical system through hybrid bonding techniques. This technology allows a lateral alignment precision of ~1 μm.[19] Because of the increased complexity of the incoupling DOE's, the sensitivity to this lateral misalignment is slightly increased in the hybrid $2F/2F$ system. This effect can be compensated for, e.g., by use of microlens–grating combinations instead of integration of all functionality in a single diffractive element.

The sensitivity of the planar optical imaging system with respect to other design parameters such as wavelength or substrate tolerances depends on the imaging configuration. Here the hybrid $2F/2F$ configuration has significant advantages over other systems. Similar imaging configurations have been previously suggested for optical computing and optical interconnections.[20,21] Figure 8 shows a hybrid imaging system in which a telecentric three-lens system is used for the imaging of the microlens planes onto each other. This system is optically equivalent to our hybrid $2F/2F$ configuration. The three lens configuration, which is used here instead of the $4F$ imaging setup to image the microlens arrays, is some-

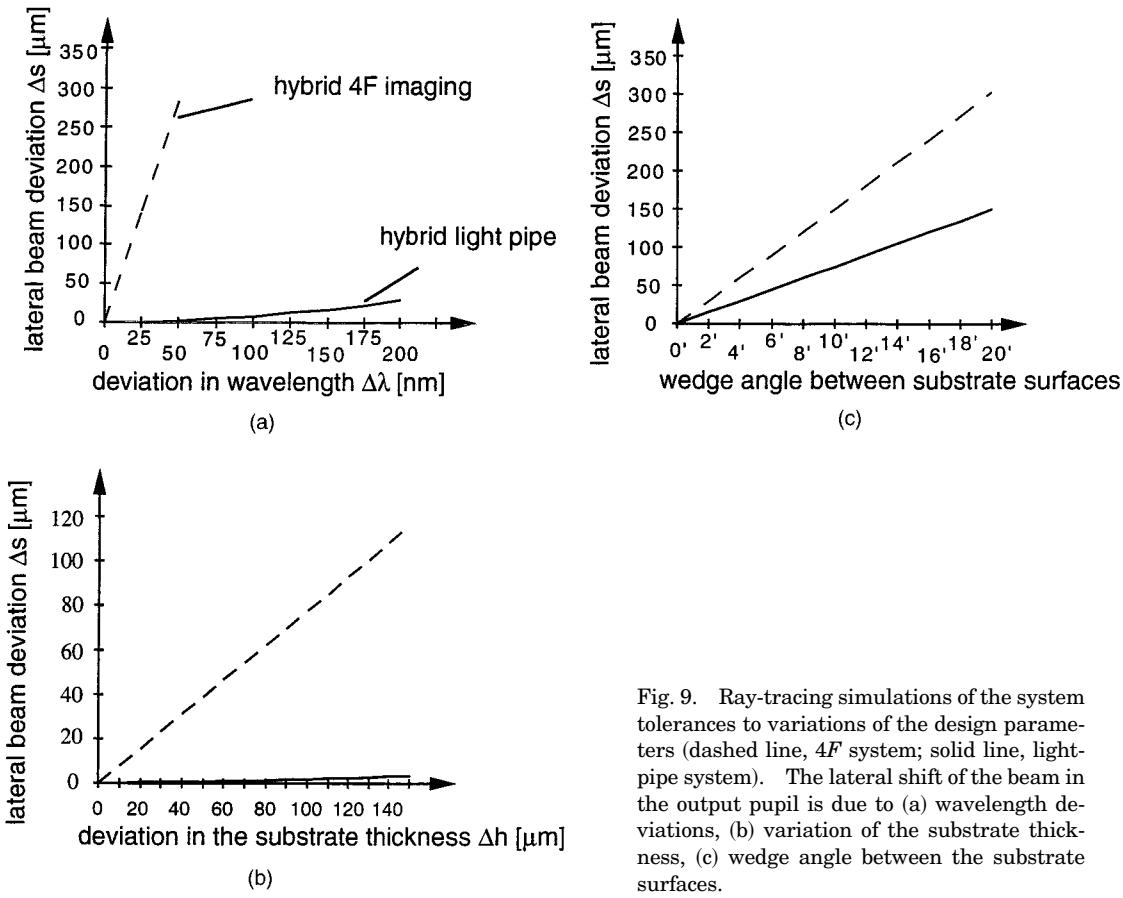

Fig. 9. Ray-tracing simulations of the system tolerances to variations of the design parameters (dashed line, 4*F* system; solid line, light-pipe system). The lateral shift of the beam in the output pupil is due to (a) wavelength deviations, (b) variation of the substrate thickness, (c) wedge angle between the substrate surfaces.

times called a light pipe. Such a configuration has already been shown to have superior imaging behavior[20] compared with that of the 4*F* setup.

It has been pointed out before that the light-pipe configuration implemented with holographic optical elements and a refractive field lens is less sensitive to chromatic errors than the 4*F* setup.[21] Here we investigate the system tolerances specifically for the planar optical system implemented with multilevel DOE's. Besides chromatic errors, we also consider the effect of errors on the substrate specifications on the imaging quality. Figure 9(a) shows ray-tracing simulations of the wavelength dependence of the lateral dislocations of a light beam after it passes through a planar optical light pipe (solid line) and a planar optical 4*F* imaging configuration (dashed line), respectively. Both setups were assumed to consist of DOE's. Clearly the influence of wavelength detuning is much more severe for the 4*F* configuration. In spite of the use of wavelength-sensitive DOE's the beam is only slightly shifted if a light pipe is used for the imaging. Similar improvements can be observed for the tolerance with respect to deviations in the substrate thickness [Fig. 9(b)] and a wedge angle between the substrate surfaces [Fig. 9(c)].

These diagrams show that a lack of parallelism of the substrate surfaces is the most significant source of beam dislocation. Nevertheless the effect can be considerably reduced if the light-pipe imaging configuration is used instead of conventional 4*F* imaging. With the use of fault-tolerant imaging configurations like the hybrid 2*F*/2*F* imaging setup, the requirements on the substrate quality and thus the manufacturing cost can be reduced significantly.

6. Hybrid 2*F*/2*F* Imaging for Space-Variant Systems

The hybrid 2*F*/2*F* imaging configuration can be used for the implementation of space-variant imaging systems that are based on regular interconnects. Figure 10, for example, illustrates how pupil division is possible with a suitable design of the microlens arrays. Now two lenses are aligned in plane L. The pupil is split in the microlens plane in order to image one half of the sources onto each of these lenses. The advantage of this configuration com-

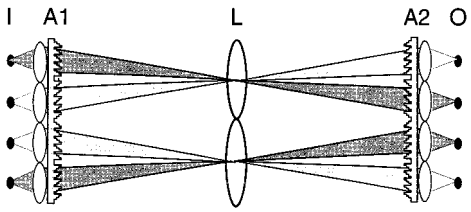

Fig. 10. Schematic of a hybrid 2*F*/2*F* configuration with divided pupil.

pared with that of the hybrid $4F$ setup is the fact that the pupil plane is located in the microlens plane. There the different channels are still separate so that no cross talk that is due to diffractive broadening is introduced. Together with magnification and demagnification this splitting of the image plane allows the implementation of, e.g., a perfect-shuffle interconnect.[22]

6. Conclusion

We demonstrated a modified hybrid imaging configuration with enhanced imaging properties. The setup is well suited for the planar optical integration because it requires only one imaging lens with a small numerical aperture. This reduces aberrations, which is especially important for the imaging along an oblique optical axis. The image quality in this configuration is constant over large image fields. The high resolution is provided by the microlenses that transmit only one single channel each. This allows the optimized design of the DOE's. Good system tolerance is achieved by the light-pipe imaging configuration. In a demonstration experiment we show that 2500 parallel data channels can be implemented in a planar optical system by adopting the hybrid $2F/2F$ imaging scheme. Estimations show that this number can be increased to arrays of O(10000) channels by use of nonsquare arrays of channels.

References

1. J. W. Goodman, F. J. Leonberger, S. Kung, and R. A. Athale, "Optical interconnections for VLSI systems," Proc. IEEE **72,** 850–865 (1984).
2. A. Huang, "Architectural considerations involved in the design of an optical digital computer," Proc. IEEE **72,** 780–786 (1984).
3. A. W. Lohmann, "Image formation of dilute arrays for optical information processing," Opt. Commun. **86,** 365–370 (1991).
4. H. S. Hinton, "Architectural considerations for photonic switching networks," IEEE J. Selected Areas Commun. **6,** 1209–1226 (1988).
5. F. B. McCormick, F. A. P. Tooley, T. J. Cloonan, J. M. Sasian, and H. S. Hinton, "Microbeam optical interconnections using microlens arrays," in *Photonic Switching*, H. S. Hinton and J. W. Goodmann, eds., Vol. 8 of OSA Proceedings Series (Optical Society of America, Washington, D.C., 1991), pp. 90–96.
6. F. Sauer, J. Jahns, C. R. Nijander, A. Y. Feldblum, and W. P. Townsend, "Refractive-diffractive micro-optics for permutation interconnects," Opt. Eng. **33,** 1550–1560 (1994).
7. F. B. McCormick, "Free space optical interconnection techniques," in *Photonics in Switching*, J. E. Midwinter, ed. (Academic, Boston, 1993).
8. J. Jahns, F. Sauer, B. Tell, K. F. Brown-Goebeler, A. Y. Feldblum, C. R. Nijander, and W. P. Townsend, "Parallel optical interconnections using surface-emitting microlasers and a hybrid imaging system," Opt. Commun. **106,** 328–337 (1994).
9. S. Sinzinger and J. Jahns, "Variations of the hybrid imaging concept for optical computing applications," in *Optical Computing*, Vol. 10 of 1995 OSA Technical Digest Series (Optical Society of America, Washington, D.C., 1995), pp. 183–185.
10. F. A. P. Tooley, S. M. Prince, M. R. Taghizadeh, F. B. McCormick, M. W. Derstine, and S. Wakelin, "Implementation of a hybrid lens," Appl. Opt. **34,** 6471–6480 (1995).
11. R. L. Morrison, "An extensible, diffractive optic system for interconnecting opto-electronic device arrays," in *Diffractive Optics and Micro-Optics*, Vol. 5 of 1996 OSA Technical Digest Series (Optical Society of America, Washington, D.C., 1996), pp. 80–82.
12. J. Jahns and A. Huang, "Planar integration of free space optical components," Appl. Opt. **28,** 1602–1605 (1989).
13. J. Jahns and B. Acklin, "Integrated planar optical imaging system with high interconnection density," Opt. Lett. **18,** 1594–1596 (1993).
14. S. Sinzinger and V. Harrison, "High-efficiency detour-phase holograms," Opt. Lett. **22,** 928–930 (1997).
15. Z. Zhou and T. J. Drabik, "Coplanar refractive–diffractive doublets for optoelectronic integrated systems," Appl. Opt. **34,** 3048–3054 (1995).
16. M. C. Hutley, P. Savander, and M. Schrader, "The use of microlenses for making spatially variant optical interconnections," Pure Appl. Opt. **1,** 337–346 (1992).
17. S. Sinzinger and J. Jahns, "Planar optics for optical interconnections in computers," in *Proceedings of the 1996 International Topical Meetings on Optical Computing and Photonics in Switching* (Optical Society of America, Washington, D.C., 1996), pp. 20–21.
18. B. Lunitz and J. Jahns, "Tolerant design of a planar optical clock distribution system," Opt. Commun. **134,** 281–288 (1997).
19. J. Jahns, R. A. Morgan, H. N. Nguyen, J. A. Walker, S. J. Walker, and Y. M. Wong, "Hybrid integration of surface-emitting microlaser chip and planar optics substrate for interconnection applications," IEEE Photon. Technol. Lett. **4,** 1369–1372 (1992).
20. K.-H. Brenner, W. Eckert, and C. Passon, "Demonstration of an optical pipeline adder and design concepts for its microintegration," Opt. Laser Technol. **26,** 229–237 (1994).
21. N. Streibl, R. Völkel, J. Schwider, P. Habel, and N. Lindlein, "Parallel optoelectronic interconnections with high packing density through a light guiding plate using grating couplers and field lenses," Opt. Commun. **99,** 167–171 (1992).
22. A. W. Lohmann, "What classical optics can do for the optical computer," Appl. Opt. **25,** 1543–1549 (1986).